Genes & Genomics (2020) 42:1151–1162
https://doi.org/10.1007/s13258-020-00985-x

Online ISSN 2092-9293
Print ISSN 1976-9571

RESEARCH ARTICLE

Molecular characterization of *Arabidopsis thaliana LSH1* and *LSH2* genes

Myungjin Lee[1] · Xiangshu Dong[2] · Hayong Song[1] · Ju Yeon Yang[1] · Soyun Kim[1] · Yoonkang Hur[1]

Received: 20 May 2020 / Accepted: 4 August 2020 / Published online: 16 August 2020

Abstract

Background *Arabidopsis thaliana* genome encodes ten DUF640 (short for domain of unknown function 640)/ALOG (short for *Arabidopsis LSH1* and Oryza G1) proteins, also known as light-dependent short hypocotyl (LSH) proteins. While some of the *LSH* genes regulate organ boundary determination and shade avoidance response, the function of most of these genes remains largely unknown.

Objective In this study, we aimed to characterize the function of *AtLSH1* and *AtLSH2* in Arabidopsis.

Methods We overexpressed *AtLSH1* and *AtLSH2* (with or without the FLAG tag) in Arabidopsis Col-0 plants under the control of the *35S* promoter. We also generated knockout or knockdown lines of these genes by miRNA-induced gene silencing (MIGS). We conducted intensive phenotypic analysis of these transgenic lines, and finally performed RNA-seq analysis of two *AtLSH2* overexpression (OX) lines.

Results Although AtLSH1 and AtLSH2 amino acid sequences showed high similarly, *AtLSH2-OX* lines showed much higher levels of their transcripts than those of *AtLSH1-OX* lines. Additionally, overexpression of *AtLSH1* and *AtLSH2* greatly inhibited hypocotyl elongation in a light-independent manner, and reduced both vegetative and reproductive growth. However, knockout or knockdown of both these *AtLSH* genes did not affect plant phenotype. Gene Ontology (GO) analysis of differentially expressed genes (DEGs) identified by RNA-seq revealed enrichment of the GO term 'response to stimulus', included phytohormone-responsive genes; however, genes responsible for the abnormal phenotypes of *AtLSH2-OX* lines could not be identified.

Conclusion Although our data revealed no close association between light and phytohormone signaling components, overexpression of *AtLSH1* and *AtLSH2* greatly reduced vegetative and reproductive growth of Arabidopsis plants. This property could be used to generate new plants by regulating expression of *AtLSH1* and *AtLSH2*.

Keywords DUF640/ALOG · AtLSH1 · AtLSH2 · Hypocotyl elongation · MIGS

Introduction

The *light-dependent* (*sensitive*) *short hypocotyl 1* (*LSH1*) gene was first identified in *Arabidopsis thaliana* as a regulator of hypocotyl elongation; overexpression of *LSH1* resulted in a hypersensitive response (short hypocotyls) in a light-dependent manner (Zhao et al. 2004). The *LSH1* gene encodes a protein with a single, small domain of unknown function (DUF640) (Yoshida et al. 2009) and a nuclear localization signal (NLS) comprising lysine and arginine residues (KKRK) (Zhao et al. 2004). The *LSH* gene family is present in all higher plants: 10 genes each in *Arabidopsis* and rice (*Oryza sativa*) (Zhao et al. 2004; Yoshida et al. 2009), 15 genes in potato (*Solanum tuberosum*) (Cho et al. 2012), and 24 genes each in *Brassica rapa* and *Brassica oleracea*

Electronic supplementary material The online version of this article (https://doi.org/10.1007/s13258-020-00985-x) contains supplementary material, which is available to authorized users.

✉ Yoonkang Hur
ykhur@cnu.ac.kr

[1] Department of Biological Sciences, College of Biological Science and Biotechnology, Chungnam National University, Daejeon 34134, Republic of Korea

[2] School of Agriculture, Yunnam University, Kunming 650091, China

(Dong et al. 2014). The plant-specific gene family encoding DUF640 proteins has been renamed as the ALOG (short for Arabidopsis LSH1 and Oryza G1) family, which is specific to land plants (Yoshida et al. 2009); however, both names (DUF640 and ALOG) are currently used interchangeably.

Based on structural analysis, the ALOG domain-containing proteins are predicted to function as transcription factors, recruiters of repressive chromatin, and/or DNA sensors in resistant proteins (Iyer and Aravind 2012). Experimental evidence suggests that ALOG proteins function as regulators of hypocotyl elongation (Zhao et al. 2004; Kwok et al. 2010; Press and Queitsch 2017; Liu et al. 2018), organ boundary determination at the shoot apical meristem (SAM), inflorescence architecture (Cho and Zambryski 2011; Takeda et al. 2011; MacAlister et al. 2012; Yoshida et al. 2013; Teo et al. 2014), and RNA-binding for phloem-mobile mRNA (Cho et al. 2012). Several studies suggest that ALOG family proteins represent an important group of regulators that affect inflorescence architecture by mediating transition from undifferentiated to differentiated cells in the SAM.

In *Arabidopsis thaliana*, *AtLSH1* (Zhao et al. 2004), *AtLSH6* (Kwok et al. 2010), and *AtLSH9* (Press and Queitsch 2017) exhibit negative effects on hypocotyl elongation; overexpression of these genes in *Arabidopsis* decreases hypocotyl length. Kwok et al. (2010) showed that overexpression of genes encoding DUF640 proteins reduces hypocotyl elongation under very low light intensity (< 20 μmol/m^2/s), thereby obstructing the shade avoidance response in plants. In rice, genes encoding DUF640 proteins *long sterile lemma* (*G1*) and *triangular hull1/beak-shaped grain 1* (*TH1/BSG1*) regulate lemma identity, grain shape, and size (Yoshida et al. 2009; Li et al. 2012; Yan et al. 2013). Together, these findings suggest that DUF640 domain-containing proteins perform diverse functions in plants.

Although *LSH* overexpression reduces hypocotyl elongation, the function of *AtLSH1* and *AtLSH2* has not yet been characterized. In this study, we examined the function both these genes by conducting gene overexpression, knockdown, and knockout analyses, phenotyping, and RNA-seq analysis.

Materials and methods

Plant materials and growth conditions

Plants of *Arabidopsis thaliana* ecotype Columbia (Col-0) were used to generate transgenic lines. Seeds were sterilized using 80% ethanol for 1 min, followed by one wash with 2% bleach solution and several washes with sterilized deionized water. The sterilized seeds were cold-stratified at 4 °C for 3 days and then sown in pots (60 × 60 mm) filled with soil. To maintain sufficient humidity for seed germination, the pots were covered by a transparent polyethylene film for the first 5–6 days. After germination, plants were grown at 22 ± 0.5 °C under long-day photoperiod (16-h light/8-h dark) and 110 μmol m^{-2} s^{-1} light intensity. To conduct in vitro experiments, seeds were sterilized with 0.1% Triton X-100 (Sigma, St. Louis, USA) and 30% bleach. After cold-stratification at 4 °C for 3 days, seeds were sown on half-strength Murashige and Skoog (1/2 MS) solid medium (Duchefa Biochemie, Haarlem, The Netherlands) supplemented with 1% sucrose and 0.8% phyto agar.

Generation of *AtLSH1* and *AtLSH2* overexpression (OX) lines

Full-length *AtLSH1* and *AtLSH2* cDNAs were cloned using gene-specific primers (Table S1), which contained *Xba*I and *Bam*HI restriction sites. The resulting fragments were cloned downstream of the cauliflower mosaic virus (CaMV) *35S* promoter in the *pCAMBIA3300* binary vector. Recombinant plasmids were introduced into *Agrobacterium tumefaciens* strain GV3101, and the transformed *Agrobacterium* cells were used to transform Col-0 plants by the floral dip method (Clough and Bent 1998). The transformants were selected on MS solid medium containing 25 mg ml^{-1} glufosinate (Sigma, St. Louis, USA) and confirmed by PCR-based genotyping using two primer sets (Table S1), one targeting the *AtLSH* gene and the other targeting the *bar* selectable marker gene. Homozygous T_3 seeds were used for subsequent experiments.

Gene expression analysis

Total RNA was isolated from rosette leaves using the TRIZOL® Reagent (Invitrogen, Carlsbad, USA). One microgram of total RNA of each sample was reverse transcribed and first-strand cDNA was synthesized using the ReverTra Ace-α kit (Toyobo, Osaka, Japan) and sequence-specific primers (Table S1). The concentration of cDNA was determined and the cDNA was diluted to 12.5 ng μl^{-1} for PCR. Semi-quantitative reverse transcription PCR (semi-RT-PCR) was performed under the following conditions: initial denaturation at 94 °C for 5 min, followed by 25 or 30 cycles of denaturation at 94 °C for 30 s, annealing at 54 °C for 30 s, and extension at 72 °C for 60 s, and a final extension at 72 °C for 7 min. The products of semi-RT-PCR were separated by electrophoresis on 1.5% agarose gels and then stained with ethidium bromide. Then, quantitative real-time PCR (qRT-PCR) was performed on the MiniOpticon system (Bio-Rad, Hercules, USA) using SYBR Green Realtime Master Mix (TOYOBO, Osaka, Japan) and the same primers that were used for semi-RT-PCR. The conditions used for qRT-PCR were as follows: initial denaturation at 95 °C for 30 s, followed by 40 cycles of denaturation at 95 °C for 5 s, annealing at 60 °C for 20 s, and extension at 72 °C for 15 s.

Fluorescence values were measured at the last step of each cycle. All analyses were performed with three biological replicates. Transcript levels of target genes were normalized relative to that of the *AtActin* gene (*AtACT*; internal reference) and analyzed using the $2^{-\Delta\Delta CT}$ method (Livak and Schmittgen 2001). Data were presented as log-transformed values of mean ± standard deviation (SD). All qRT-PCR analyses were carried out in three biological replicates, each containing three technical replicates.

Measurement of hypocotyl length

Sterilized and cold-stratified seeds were sown in 12 × 12 cm square Petri dishes (with grids) containing 1/2 MS medium. After seed germination, the plates were exposed to white light for 7 h before being transferred to different light conditions. Monochromatic light sources were obtained from a light emission diode (LED) facility (Plant LED Illumination System GF-520, Koyang city, South Korea). Cool white fluorescent lamps were used as the source of white light. The intensity of red light (cR) and far-red light (cFR) was 10 µmol m^{-2} s^{-1}. Images of 10 seedlings of each line were captured and scanned into a computer, and hypocotyl lengths were measured using the Image Tool Program (www.ansci.wisc.edu/equine/parrish/index.html).

Measurement of vegetative growth and reproductive capacity

Arabidopsis plants transformed with the empty vector (control) and those overexpressing *AtLSH1* and *AtLSH2* were grown in 2.5 × 2.5 inch pots under the abovementioned conditions. At 30 days after germination (DAG), vegetative growth parameters of 15 individual plants of each genotype were measured and expressed as mean ± SD. Additionally, two siliques were collected from each of the 15 plants, and seed number and silique length were quantified.

Analysis of AtLSH1 and AtLSH2 protein levels in OX lines

To generate Arabidopsis plants overexpressing FLAG-tagged AtLSH1 and AtLSH2 proteins, coding sequences of *AtLSH1* and *AtLSH2* were amplified from Col-0 cDNA by PCR using gene-specific primers (*AtLSH1*_forward: 5′-ATCTAAACTAGTATGGATTTGATCTCA-3′, *AtLSH1*_reverse: 5′-ATATAAGAGCTCTACTGTTGCACCC-3′; *AtLSH2*_forward: 5′-ATCTAAACTAGTATGGATTTGATCTCA-3′, *AtLSH2*_reverse: 5′- AGTTATGAGCTCTTGAGTTGCACCGT- 3′; the underlined sequences in the forward and reverse primers represent *Spe*I and *Sac*I restriction sites, respectively). The PCR products were cloned into the *pCR_CCD* vector derived from the *pCR8/GW/TOPO* entry vector (Invitrogen, Carlsbad, USA). The resulting *AtLSH1* and *AtLSH2* inserts were cloned into the *pBIB-BAR*$^{+}$*-35S-FLAG* destination vector (Guo et al. 2010) using LR recombinase (Invitrogen, Carlsbad, USA). The resulting constructs were introduced into Col-0 plants by *Agrobacterium*-mediated transformation using the floral dip method (Clough and Bent 1998). The transformants were initially selected by spraying with 0.1% BASTA herbicide and then confirmed by PCR-based genotyping. Several individual lines harboring a single T-DNA locus were selected, based on the segregation ratio (basta resistant: sensitive = 3:1).

To perform western blotting, total proteins on 10% polyacrylamide gels were separated by sodium dodecyl sulfate–polyacrylamide gel electrophoresis (SDS–PAGE) and transferred onto polyvinylidene difluoride (PVDF) membranes. To visualize the transfer efficiency, membranes were stained with Coomassie Brilliant Blue. Blots were incubated with anti-FLAG antibodies (1:1,000 dilution) in TBST (20 mM Tris–HCl [pH 7.6], 127 mM NaCl, and 0.1% Tween20) at 4 °C for 1 h. Subsequently, blots were washed five times with TBST and then incubated with HRP-conjugated secondary antibody (1:10,000 dilution) in TBST at 4 °C for 1 h. HRP signals were detected using PicoEPD™ Western Reagent (ELPISbio, Daejeon, Korea) and Chemiluminescence CCD Imaging System (Atto, Tokyo, Japan).

Gene knockout by miRNA-induced gene silencing (MIGS)

The MIGS technology (de Felippes et al. 2012) was used to specifically knockout *AtLSH1* and *AtLSH2* expression. The forward primer specific to either *AtLSH1* or *AtLSH2* contained a 24-nt sequence of miR173 and the 3′ region of the corresponding *AtLSH* gene. The *AtLSH1* and *AtLSH2* sequences used for the constructs were 324 nt (3′-225 + 3′-UTR 99 nt) and 420 nt (3′-271 + 3′-UTR 131 nt), respectively. The resulting fragments were cloned into the *pCAMBIA3300* vector and then transformed into Col-0 plants (as described above). The phenotype of transgenic plants and expression level of *AtLSH1* and *AtLSH2* genes were subsequently analyzed.

Phylogenetic analysis

Sequences of all 10 Arabidopsis LSH proteins (AtLSH1–AtLSH10) were obtained from the National Center for Biotechnology Information (NCBI; https://ncbi.nlm.nih.gov/nucelotide). Amino acid sequence alignment and phylogenetic tree construction were performed using the "build" function of ETE3 v3.1.1 (Huerta-Cepas et al. 2016), as implemented in GenomeNet (https://www.genome.jp/tools/ete/). The phylogenetic tree was constructed using FastTree v2.1.8, with default parameters (Price et al. 2009).

RNA-seq analysis of *AtLSH2-OX* lines

Shoots of wild-type (WT; Col-0) plants and *AtLSH2-OX* lines (*AtLSH2-OX1* for severe abnormal phenotype and *AtLSH2-OX4* for no or mild abnormal phenotype) were harvested at 7 DAG (seedling stage) and 18 DAG (bolting initiation stage). Total RNA was isolated from each sample using the TRIZOL® Reagent (Invitrogen, Carlsbad, USA) and treated with RNase-free DNase (Promega, Madison, USA) to remove genomic DNA contamination. The quantity and integrity of total RNA samples were checked using NanoDrop spectrophotometer (NanoDrop Technologies, Waltham, USA) and an Agilent 2100 BioAnalyzer (Agilent Technologies, Santa Clara, USA). Total RNA samples with an RNA integrity number (RIN) > 7 were used to prepare RNA-seq libraries. A total of six RNA-seq libraries were constructed using TruSeq RNA Library Prep Kit (Illumina Inc. San Diego, USA) by SEEDERS (Daejeon, South Korea) and sequenced on the Illumina HiSeq 2000 platform (Illumina Inc.). Short transcriptome reads were preprocessed using DynamicTrim and LenghSort of SolexQA package (Cox et al. 2010). Then, RNA-seq data were analyzed according to the method described by Trapnell et al. (2012). Gene ontology (GO) enrichment analysis was carried out using agriGO (Tian et al. 2017) and the results were visualized using the R package in the clusterProfiler software version 3.8 (Yu et al. 2012).

Results

Sequence analysis of AtLSH proteins

To predict the function of AtLSH1 and AtLSH2, we aligned the amino acid sequences of all 10 AtLSHs using CLUSTALW (https://www.genome.jp/tools-bin/clustalw) and conducted phylogenetic analysis. The results of phylogenetic analysis revealed that AtLSHs grouped into two clades, one comprising six AtLSHs (AtLSH1–AtLSH6) and the other comprising four AtLSHs (AtLSH7–AtLSH10) (Fig. 1a). Grouping of AtLSH1 and AtLSH2 into the same clade implies that these proteins perform similar physiological functions. Multiple sequence alignment showed that all 10 AtLSHs contain four helices, a zinc-ribbon domain (commonly found in DNA-binding proteins and transcription factors), and an NLS (KKRK/KRKR) (Fig. 1b). These features suggest that AtLSHs function as transcription factors in the nucleus.

Characterization of *AtLSH1* and *AtLSH2* OX lines

To elucidate function of *AtLSH1* and *AtLSH2*, both genes were overexpressed in Arabidopsis under the control of the CaMV *35S* promoter. Five independent homozygous T_3 lines overexpressing *AtLSH1* or *AtLSH2* were selected, and the 5th leaf of each line was used to analyze leaf morphology and *AtLSH1* or *AtLSH2* transcript level (Fig. 2). Transgenic lines showed abnormal leaf phenotypes (such as short blade length and undulated margins) compared with the WT. The severity of these abnormal leaf phenotypes was proportional to the transcript level of *AtLSH1* or *AtLSH2*. Interestingly, relative transcript levels of overexpressed *AtLSH* genes were higher in *AtLSH2-OX* lines than in *AtLSH1-OX* lines.

To determine whether relative transcript levels correlate with protein levels, we generated *AtLSH-FLAG* OX lines, and characterized their leaf morphology, transcript levels, and protein levels (Fig. 3). Plants showing strong and mild abnormalities in leaf morphology exhibited relatively high levels of *AtLSH1* and *AtLSH2* transcripts and corresponding proteins, supporting a direct correlation between relative transcript and protein levels. In addition, plants producing higher levels of *AtLSH1* or *AtLSH2* transcripts and its corresponding proteins showed more severe abnormal leaf phenotypes. Additionally, the level of *AtLSH2* expression in *AtLSH2-OX* plants was generally higher than that of *AtLSH1* expression of *AtLSH1-OX* plants. Plants showing normal leaf phenotypes showed very low levels of *AtLSH1* and *AtLSH2* transcripts and undetectable levels of the corresponding proteins.

AtLSH1 and *AtLSH2* overexpression reduced hypocotyl elongation

A previous study showed that *AtLSH1* overexpression reduces hypocotyl elongation in a light-dependent manner (Zhao et al. 2004). To extend this finding, we examined hypocotyl elongation in transgenic and WT plants treated with white light (cW), red light (cR), far-red light (cFR), and darkness for 5 days (Fig. 4). Except *AtLSH1-OX5*, all transgenic lines showed a reduction in hypocotyl elongation under various light treatments (*AtLSH1-OX* lines: 33% reduction in cW, 25% in cFR, 30% in cR, and 25% in dark; *AtLSH2-OX* lines: 45% reduction in cW, 38% in cFR, 55% in cR, and 62% in dark). The reduction in hypocotyl length was more dramatic in *AtLSH2-OX* lines than in *AtLSH1-OX* lines, which was consistent with transgene expression levels (Fig. 2). Notably, hypocotyl length was decreased not only under light but also in the dark in all transgenic lines, suggesting that this reduction in hypocotyl elongation was independent of light.

AtLSH1 and *AtLSH2* overexpression decreased plant growth and development

AtLSH1-OX and *AtLSH2-OX* lines were grown in 2.5-inch pots under long-day (16-h light/8-h dark) condition with

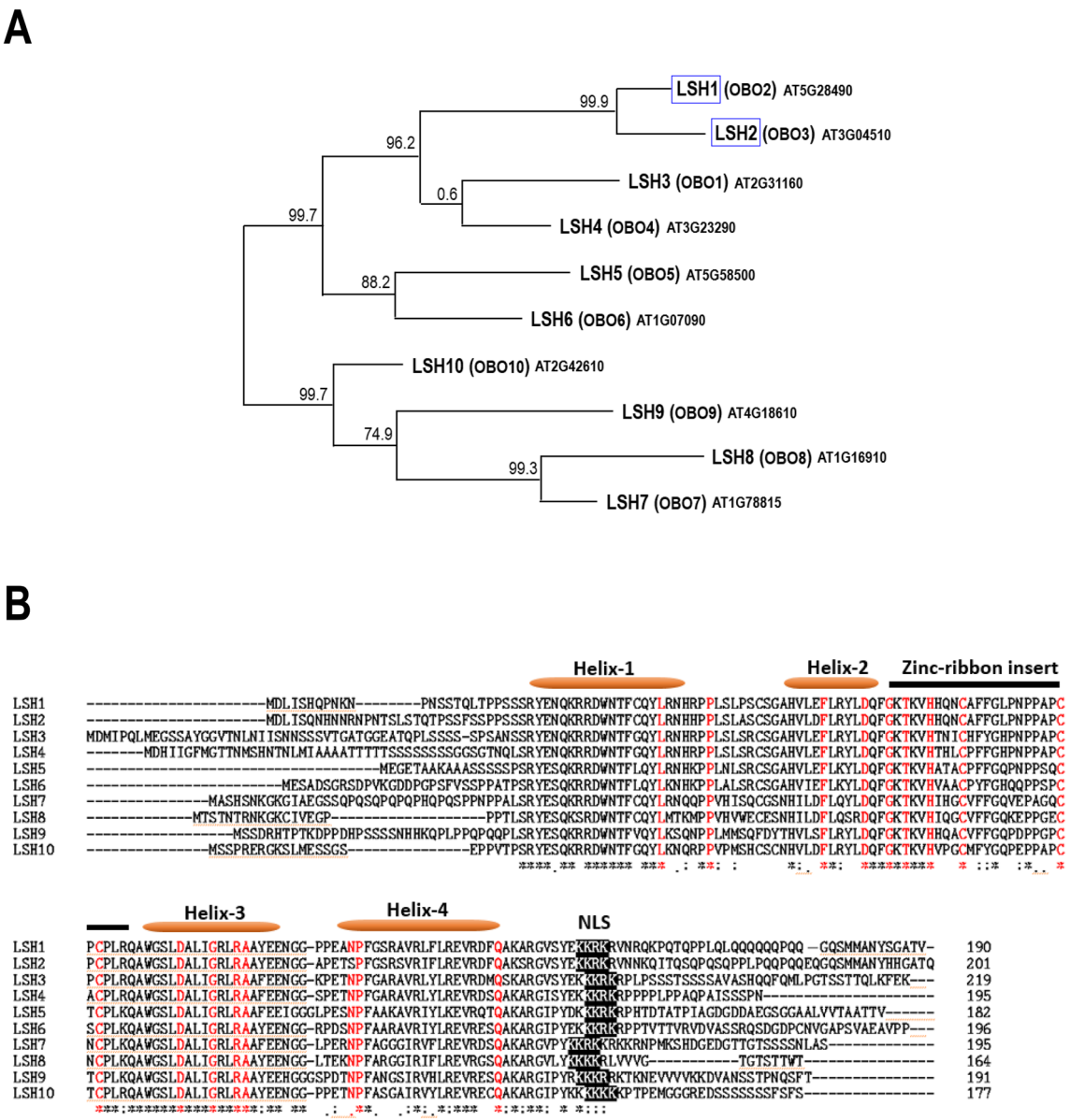

Fig. 1 Phylogenetic analysis and amino acid sequence alignment of 10 *Arabidopsis thaliana* LSH proteins. **a** Phylogenetic analysis. OBO, ORGAN BOUNDARY (Cho and Zambryski 2011). **b** Amino acid sequence alignment. Amino acid residues shown in red are conserved among XerC/D-like proteins, protelomerases, topoisomerase-IA, Flp-tyrosine recombinases, and DUF640/ALOG proteins (Iyer and Aravind 2012). *NLS* nuclear localization signal (color figure online)

a photon flux density of 110 µmol m^{-2} s^{-1}. We monitored the growth of these plants during both vegetative and reproductive phases (Tables 1 and 2). Transgenic *AtLSH1-OX* and *AtLSH2-OX* lines showed a substantial reduction in vegetative growth and reproductive capacity compared with plants transformed with the *pCAMBIA3300* empty vector (control). The reduction in vegetative and reproductive growth was more pronounced in *AtLSH2-OX* lines than in *AtLSH1-OX* lines.

Phenotypic analysis of *AtLSH1* and *AtLSH2* knockdown lines

To knockout or knockdown the expression of *AtLSH1* and *AtLSH2* specifically, we applied the MIGS technology (de Felippes et al. 2012) using miR173 (Fig. 5). The sequence identity between *AtLSH1* (324 nt) and *AtLSH2* (402 nt) attached to miR173ts (target site) was only 51% (Fig. 5a), thereby ensuring no cross-reactivity in gene silencing. MIGS

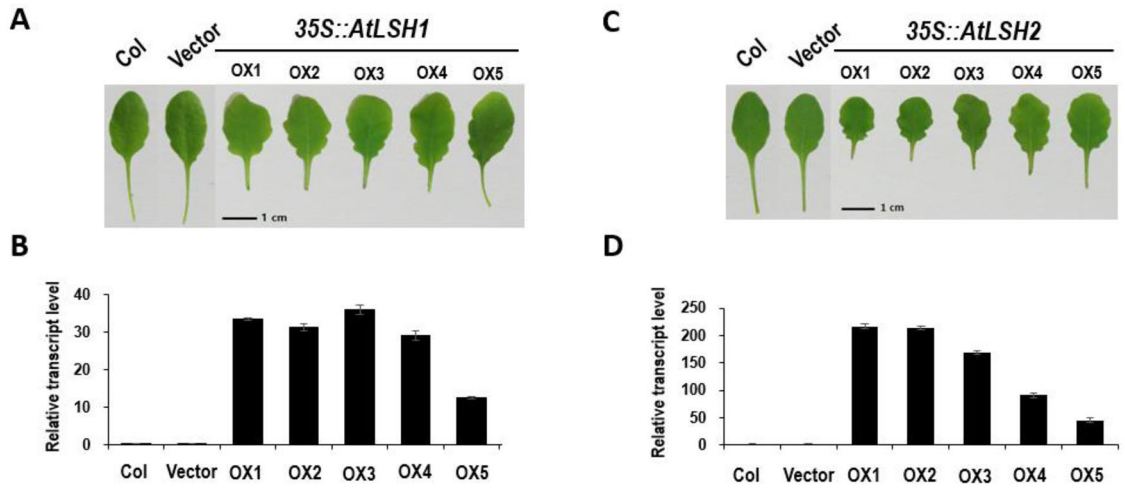

Fig. 2 Phenotypic and molecular characterization of *AtLSH1* and *AtLSH2* overexpression (OX) lines. **a**–**d** Leaf morphology (**a**, **c**) and expression analysis (**b**, **d**) of *AtLSH1-OX* and *AtLSH2-OX* lines. The 5th leaf of each plant was selected for phenotypic and gene expression analyses. Transcript levels of *AtLSH* genes were normalized relative to those of the *AtActin* (*AtACT*) gene. Col, wild-type; vector, empty vector control; OX1–OX5, independent overexpression lines

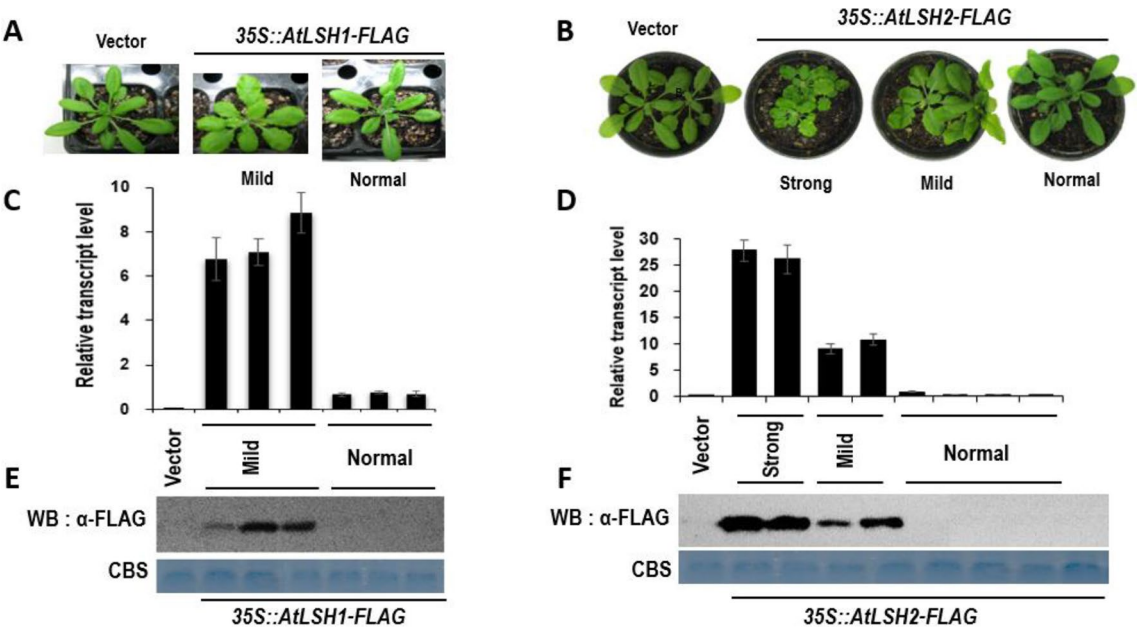

Fig. 3 Phenotypic and molecular characterization of T_2 plants expressing FLAG-tagged *AtLSH1* and *AtLSH2*. **a**, **b** Phenotypic variability among *AtLSH1-FLAG* (**a**) and *AtLSH2-FLAG* (**b**) transgenic plants. Vector represents the *pBIB-35S-FLAG* empty vector control; mild and normal indicate the leaf phenotype. **c**, **d** Expression analysis of *AtLSH1* (**c**) and *AtLSH2* (**d**) by quantitative real-time PCR (qRT-PCR). Transcript levels of *AtLSH* genes were normalized relative to those of *AtACT*. **e**, **f** Western blotting analysis of plants shown in (**b**, **c**). Proteins were detected using an anti-FLAG antibody (α-FLAG) (top), and Coomassie blue staining (CBS) of RuBisCo was used as a loading control (bottom). All analyses were conducted using the 5th leaf of 28-day-old plants

plants in the T_1 generation showed no phenotypic differences compared with plants transformed with the *pCAMBIA3300-35S* empty vector (control), which was consistent with *AtLSH1* and *AtLSH2* transcript levels. The *atlsh1* and *atlsh2* knockout mutant lines showed no phenotypic differences compared with the control (data not shown), which is consistent with the results of T-DNA insertion mutants (Zhao et al. 2004).

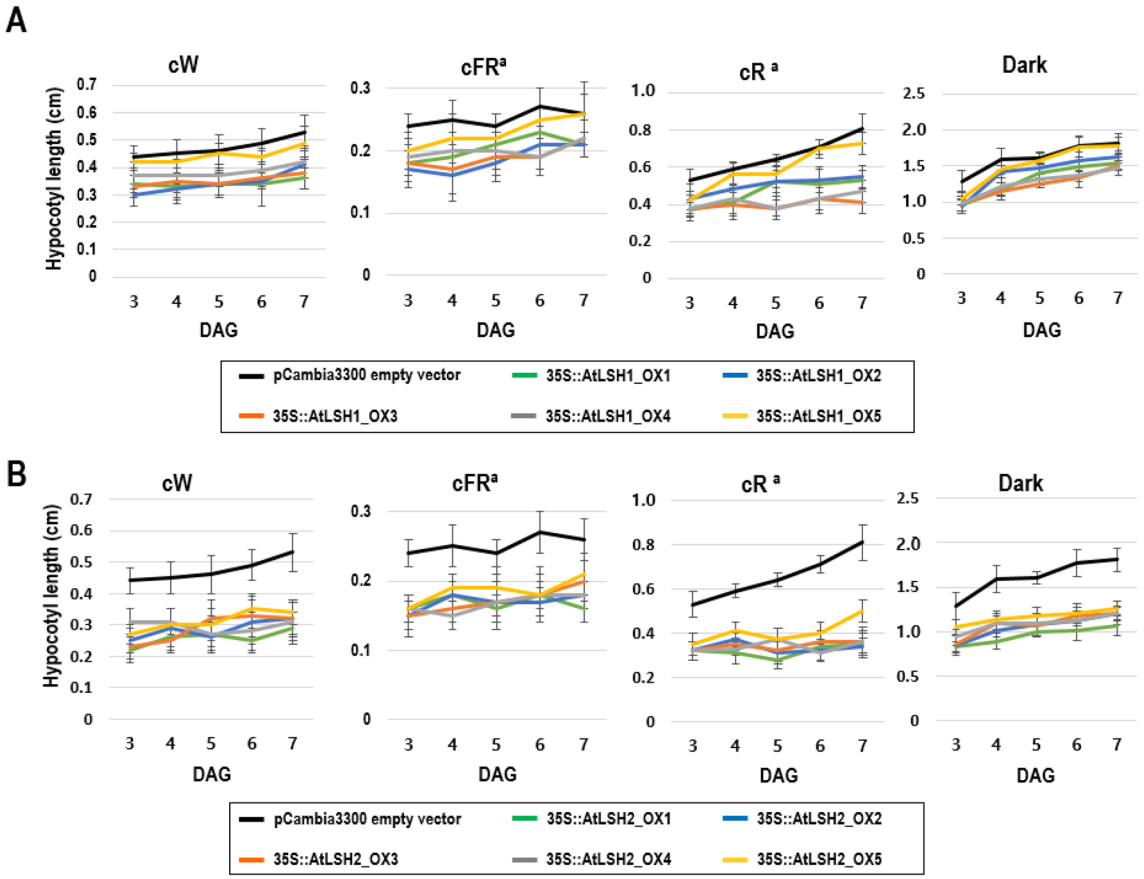

Fig. 4 Hypocotyl elongation of *AtLSH1-OX* and *AtLSH2-OX* lines under different light conditions. **S**eedlings were exposed to light or darkness for 8 days. Under each light condition, images of 10 seedlings of each OX line and the pCAMBIA3300 empty vector control were scanned into a computer and hypocotyl length was measured using the Image Tool program (www.ansci.wisc.edu/equine/parrish/index.html). [a]Fluence rate, 10 µmol m^{-2} s^{-1}. *cW* white light, *cR* red light, *cFR* far-red light, *DAG* days after germination

Table 1 Summary of vegetative and reproductive growth characteristics of soil-grown *AtLSH1* overexpression (OX) lines and the empty vector control

Trait	Control[†]	*AtLSH1-OX* lines[†]				
		OX1	OX2	OX3	OX4	OX5
Plant height (cm)	5.6 ± 0.7	4.9 ± 0.4	4.7 ± 0.5	4.7 ± 0.4	4.4 ± 0.5	5.3 ± 0.5
Primary shoot length (cm)	20.6 ± 1.4	16.2 ± 1.7	16.5 ± 1.9	17.8 ± 1.6	17.4 ± 1.3	18.5 ± 1.8
No. of lateral shoots	4.7 ± 0.8	3.2 ± 0.8	3.3 ± 0.5	3.4 ± 0.5	3.2 ± 0.4	4.0 ± 0.8
No. of leaves per plant	9.3 ± 0.7	7.6 ± 0.5	7.4 ± 0.6	7.2 ± 0.8	7.2 ± 0.6	8.7 ± 0.6
Length of mature silique (cm)	1.3 ± 0.07	1.0 ± 0.11	1.0 ± 0.14	1.1 ± 0.06	1.1 ± 0.14	1.1 ± 0 .08
No. of seeds per silique[§]	53.9 ± 6.3	32.7 ± 3.5	39.3 ± 6.2	40.9 ± 4.8	41.9 ± 5.5	46.9 ± 5.5
No. of siliques per primary shoot	68.0 ± 4.8	48.9 ± 4.0	43.9 ± 4.3	47.0 ± 4.0	48.3 ± 2.1	51.9 ± 3.2

[†]Data represent the mean ± standard deviation (SD; $n = 15$)

[§]This value was determined based on the number of seeds in two siliques harvested from each of the 15 plants

RNA-seq analysis of *AtLSH2-OX* lines

To identify genes responsible for the abnormal leaf phenotypes of *AtLSH-OX* lines, we performed RNA-seq analyses of WT (Col-0) plants and two *AtLSH2-OX* lines (*AtLSH2-OX1* and *AtLSH2-OX4*) using shoot samples collected at 7 and 18 DAG. Paired-end sequencing generated a total of 217,672,390 reads, with approximately 19 billion nucleotides (Table S2). A total of 27,416 representative Arabidopsis transcripts were obtained by comparison

Table 2 Summary of vegetative and reproductive growth characteristics of soil-grown *AtLSH2-OX* lines and the empty vector control

Trait	Control†	*AtLSH2-OX* lines†				
		OX1	OX2	OX3	OX4	OX5
Plant height (cm)	5.1 ± 0.4	1.9 ± 0.1	2.1 ± 0.2	3.8 ± 0.4	3.4 ± 0.3	4.3 ± 0.4
Primary shoot length (cm)	21.9 ± 1.3	8.1 ± 1.5	12.9 ± 1.4	19.9 ± 1.3	20.0 ± 1.1	17.0 ± 1.7
No. of lateral shoots	4.9 ± 0.6	2.2 ± 0.4	2.2 ± 0.4	2.2 ± 0.4	2.5 ± 0.5	3.9 ± 0.7
No. of leaves per plant	9.0 ± 0.8	6.5 ± 1.0	6.1 ± 0.6	6.2 ± 04	6.1 ± 0.4	8.4 ± 0.7
Length of mature silique (cm)	1.2 ± 0.06	0.4 ± 0.09	0.4 ± 0.05	0.8 ± 0.05	0.8 ± 0.03	1.1 ± 0.09
No. of seeds per silique§	52.5 ± 6.5	7.7 ± 3.8	7.2 ± 3.5	21.9 ± 4.4	25.5 ± 3.8	40.7 ± 5.0
No. of siliques per primary shoot	70.5 ± 6.5	5.6 ± 1.7	6.2 ± 2.5	48.5 ± 5.4	46.2 ± 5.8	55.0 ± 2.9

†Data represent the mean ± SD ($n = 15$)

§This value was determined based on the number of seeds in two siliques harvested from each of the 15 plants

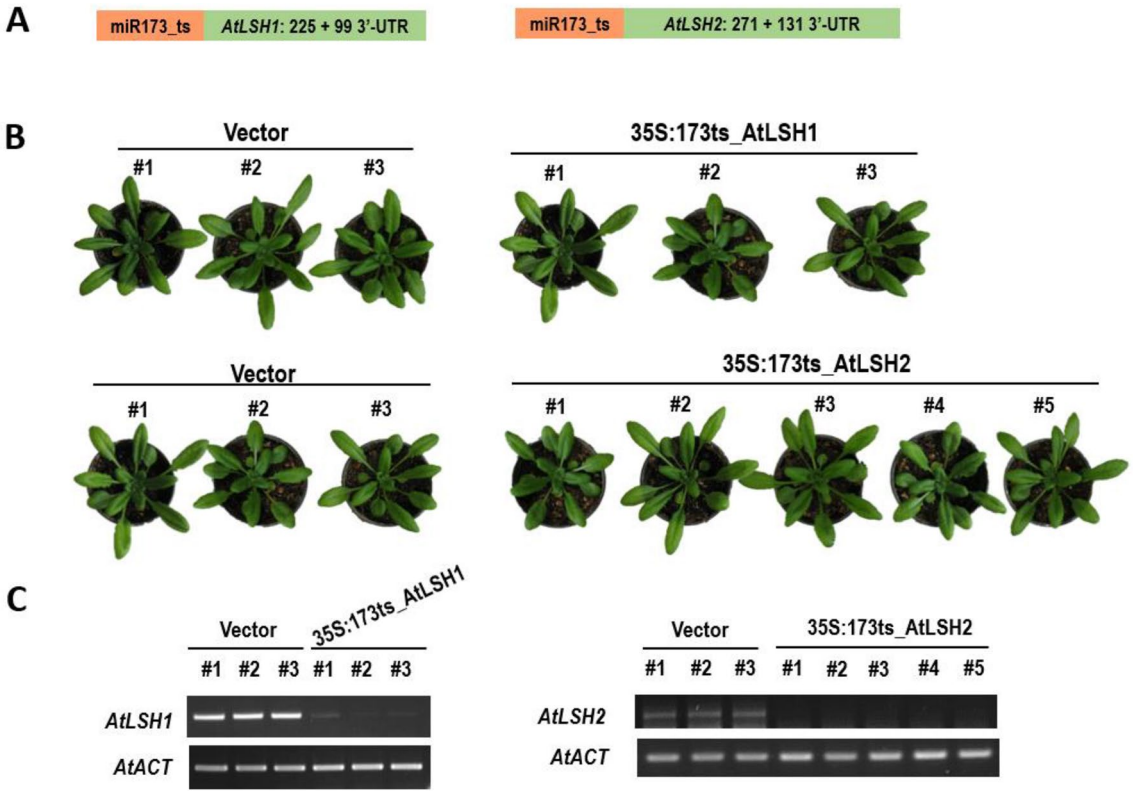

Fig. 5 Inhibition of *AtLSH1* and *AtLSH2* expression by miRNA-induced gene silencing (MIGS). **a** Schematic representation of MIGS constructs. **b** Images showing the phenotype of 35S:173ts_AtLSH1 and 35S:173ts_AtLSH2 plants. **c** Expression analysis of *AtLSH1* and *AtLSH2* by semi-quantitative reverse transcription PCR (RT-PCR)

with TAIR10 reference genes (https://phytozome.jgi.doe.gov) (Table S3). Transcript levels of *AtLSH3–AtLSH10* showed no significant differences between transgenic and WT plants (Table 3). Transcript levels of *AtLSH1* were increased in transgenic lines compared with WT plants, but not as much as those of *AtLSH2* transcripts. These data imply that abnormal leaf phenotypes and reduced hypocotyl elongation of transgenic plants were caused by *AtLSH1* or *AtLSH2* overexpression, resulting in altered expression levels of other genes.

Next, we performed GO enrichment analysis of differentially expressed genes (DEGs) (Fig. 6). GO terms such as 'response to stimulus', 'response to stress', and 'iron ion binding' were enriched among genes upregulated in *AtLSH2-OX* lines. 'Response to stimulus' included 19 genes highly responsive to phytohormones, biotic and abiotic

Table 3 Expression of *AtLSH* genes in *AtLSH2-OX* lines and Col-0 plants analyzed by RNA-seq at 7 and 18 days after germination (DAG)

Gene	Locus_ID	7 DAG (TPM)†			18 DAG (TPM)†		
		Col-0	*AtLSH2-OX4*	*AtLSH2-OX1*	Col-0	*AtLSH2-OX4*	*AtLSH2-OX1*
LSH1	AT5G28490	16	621	1,639	64	305	497
LSH2	AT3G04510	4	59,733	151,321	12	27,014	55,085
LSH3	AT2G31160	24	33	19	56	36	22
LSH4	AT3G23290	60	95	103	198	162	153
LHS5	AT5G58500	7	10	4	10	4	3
LSH6	AT1G07090	94	108	148	63	40	37
LSH7	AT1G78815	3	1	3	2	1	1
LSH8	AT1G16910	3	1	3	2	3	3
LSH9	AT4G18610	7	10	6	9	4	3
LHS10	AT2G42610	65	42	68	316	205	160

†Data are expressed as Transcripts Per Kilobase Million (TPM) values

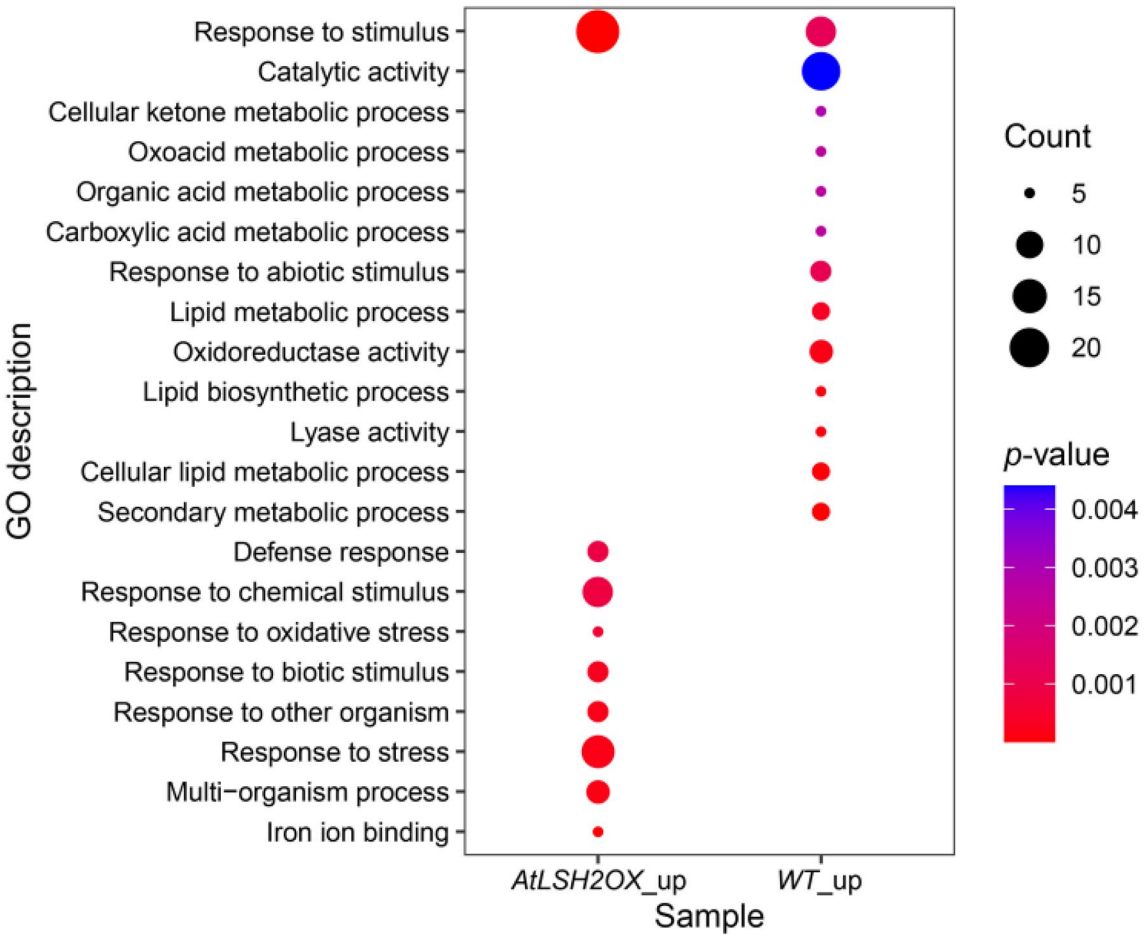

Fig. 6 Gene ontology (GO) enrichment analysis of genes upregulated or downregulated (WT_up) in *AtLSH2-OX* lines relative to the wild type (WT). GO enrichment analysis was performed using agriGO (Tian et al. 2017) and the results were visualized using the R package in the clusterProfiler software version 3.8 (Yu et al. 2012)

stresses, and disease resistance (Table S4), implying that the extremely high levels of AtLSH2 would be similar to harsh condition for plant growth. Secondary metabolic process and lipid metabolic process were enriched among genes downregulated in *AtLSH2-OX* lines. The downregulated genes included *ACP2* (which encodes ACC oxidase 2) (Ramadoss

et al. 2018) and *MYBL2* (which encodes MYB-like 2) (Nguyen et al. 2015), possibly resulting in the reduction of abiotic stress resistance. Unfortunately, we could not identify genes leading to abnormal leaf phenotypes and reduction in hypocotyl elongation by RNA-seq analysis.

Discussion

AtLSH1 and AtLSH2 clustered in the same subclade (Fig. 1), and overexpression of *AtLSH1* and *AtLSH2* genes in Arabidopsis caused abnormal leaf morphology. The severity of the abnormal leaf phenotype was associated with the levels of *AtLSH1* and *AtLSH2* transcripts and those of the corresponding proteins (Figs. 2 and 3). The *AtLSH1-OX* and *AtLSH2-OX* lines also showed a great reduction in vegetative growth and reproductive capacity compared with the control (Tables 1 and 2). Hypocotyl elongation was greatly inhibited by overexpression of *AtLSH1* and *AtLSH2*, although the reduction in hypocotyl elongation was not dependent on light (Fig. 4). We performed RNA-seq analysis to identify key genes responsible for the abnormal leaf morphology and reduced hypocotyl elongation in *AtLSH2-OX* lines; however these genes could not be identified since the DEGs did not include genes involved in leaf development or differentiation (Tsukaya 2013). Additionally, we could not explain why transcript levels in *AtLSH2-OX* lines were much higher than those in *AtLSH1-OX* lines, and why knockout of *AtLSH1* and *AtLSH2* caused no phenotypic changes. Together, these data suggest that AtLSH1 and AtLSH2 perform dramatic functions that remain unknown. Two transgenic lines, *AtLSH1-OX5* and *AtLSH2-OX5*, which showed low transgene expression, could be used to generate low-light tolerant plants, similar to that suggested by Kwok et al. (2010).

Among various plant growth processes, hypocotyl elongation has attracted much attention because the hypocotyl is a simple organ and light and phytohormones affect its elongation (Vandenbussche et al. 2005). Generally, auxin and gibberellin (GA) stimulate hypocotyl elongation, whereas abscisic acid (ABA) and light repress hypocotyl elongation. In the absence of light, phytochrome-interacting factor (PIF) proteins (PIF1, PIF3, PIF4, and PIF5) accumulate in the nucleus and inhibit photomorphogenesis (Shin et al. 2009). PIF4 interacts with AUXIN RESPONSE FACTORS (ARFs) ARF6, ARF7, and ARF8 to stimulate hypocotyl elongation (Oh et al. 2014; Reed et al. 2018). Auxin induces the degradation of ARF inhibitor proteins, AUX/IAA (Chapman and Estelle 2009; Vernoux et al. 2011), thereby promoting hypocotyl elongation in the dark. GA promotes hypocotyl elongation by stimulating the degradation of DELLA repressor proteins (Alabadí et al. 2004). By contrast, ABA suppresses hypocotyl elongation by inhibiting an auxin-induced plasma membrane H^+-ATPase (Hayashi et al. 2014). ABA-responsive genes also repress shade avoidance response-driven hypocotyl elongation (Kohnen et al. 2016). Recently, Lorrai et al. (2018) showed that ABA suppresses hypocotyl elongation by acting on GA metabolic genes; this increases the level of DELLA proteins (GAI and RGA), which affects GA signaling and ultimately represses auxin biosynthetic genes. In this study, *AtLSH1-OX* and *AtLSH2-OX* lines showed a reduction in hypocotyl elongation not only under light but also in the dark (Fig. 4). Putative regulator genes associated with signaling of the abovementioned phytohormones were not differentially expressed between *AtLSH2-OX* lines and WT plants (Table S3). This suggests that suppression of hypocotyl elongation in *AtLSH1-OX* and *AtLSH2-OX* lines was caused by an unknown mechanism.

Although the precise functions of DUF640/ALOG proteins have not yet been identified, these proteins play four possible roles, based on published information: regulation of inflorescence architecture, determination of organ identity and differentiation, transport of mRNA, and regulation of hypocotyl elongation. *ALOG* genes control inflorescence architecture in rice and tomato (Yoshida et al. 2009, 2013; Li et al. 2012; MacAlister et al. 2012; Yan et al. 2013; Teo et al. 2014). In Arabidopsis, *ALOG* genes are expressed at the boundary region of the SAM and lateral organs, indicating their function in organ identity (Cho and Zambryski 2011; Takeda et al. 2011). Moreover, sequence analysis of ALOG proteins suggests that these proteins help establish organ identity and differentiation by binding to specific DNA sequences and acting as transcription factors or repressive chromatin recruiters (Iyer and Aravind 2012). The current study supports the notion that all *LSH* genes are involved in leaf formation and determination of the boundary between the leaf and stem, as shown in Fig. 2a and c as well as in Fig. 3a and b. In potato, *StLSH10* encodes an RNA-binding protein (B5RBP3), which binds to the 3′ untranslated region (3′UTR) of *StBEL5*, a mobile mRNA that controls tuber formation (Cho et al. 2012; Lin et al. 2013). *StBEL5* mRNA is highly abundant in petioles, where it moves long distances through the phloem (Cho et al. 2012). RNA-binding proteins are commonly detected in companion cells and sieve elements of leaf veins, where they serve as chaperones of mobile mRNAs. Transcript levels of *StLSH10* are remarkably low in leaves but extremely high in petioles, stolons, and young tubers, suggesting that the B5RBP3 protein is involved in mRNA transport and tuber development (Cho et al. 2012). The *LSH* genes of *Brassica* species showed an expression pattern similar to that of *StLSH10* (Dong et al. 2014; Lee et al. 2020). However, our transcriptome analysis did not reveal mRNAs involved in long-distance transport. To elucidate the function of AtLSH proteins, yeast two-hybrid and three-hybrid experiments should be performed in future studies.

Acknowledgements This work was supported by a grant from the Basic Science Research Program through the National Research Foundation of Korea (NRF) funded by the Ministry of Education (NRF-2014068885), Republic of Korea.

Compliance with ethical standards

Conflict of interest The authors declare no conflict of interest.

References

Alabadí D, Gil J, Blázquez MA, García-Martínez JL (2004) Gibberellins repress photomorphogenesis in darkness. Plant Physiol 134:1050–1057

Chapman EJ, Estelle M (2009) Mechanism of auxin-regulated gene expression in plants. Annu Rev Genet 43:265–285

Cho E, Zambryski PC (2011) Organ boundary1 defines a gene expressed at the junction between the shoot apical meristem and lateral organs. Proc Natl Acad Sci USA 108:2154–2159

Cho SK, Kang IH, Carr T, Hannapel DJ (2012) Using the yeast three-hybrid system to identify proteins that interact with a phloem-mobile mRNA. Front Plant Sci 3:189

Clough SJ, Bend AF (1998) Floral dip: a simplified method for *Agrobacterium*-mediated transformation of *Arabidopsis thaliana*. Plant J 16:735–743

Cox MP, Peterson DA, Biggs PJ (2010) SolexaQA: At-a-glance quality assessment of Illumina second-generation sequencing data. BMC Bioinform 11:485

De Felippes FF, Wang JW, Weigel D (2012) MIGS: miRNA-induced gene silencing. Plant J 70:541–547

Dong X, Lee J, Nou IS, Hur Y (2014) Expression characteristics of *LSH* genes in *Brassica* suggest their applicability for modification of leaf morphology and the use of their promoter for transgenesis. Plant Breed Biotechnol 2:126–138

Guo X, He K, Yang H, Yuan T, Lin H, Clouse SD, Li J (2010) Genome-wide cloning and sequence analysis of leucine-rich repeat receptor-like protein kinase genes in *Arabidopsis thaliana*. BMC Genom 11:19

Ha CM, Jun JH, Nam HG, Fletcher JC (2007) *BLADE-ON-PETIOL1* and *2* control *Arabidopsis* lateral organ fate through regulation of LOB domain and adaxial-abaxial polarity genes. Plant Cell 19:1809–1825

Hayashi Y, Takahashi K, Inoue S, Kinoshita T (2014) Abscisic acid suppresses hypocotyl elongation by dephosphorylating plasma membrane $H^{(+)}$-ATPase in *Arabidopsis thaliana*. Plant Cell Physiol 55:845–853

Huerta-Cepas J, Serra F, Bork P (2016) ETE 3: Reconstruction, analysis, and visualization of phylogenomic data. Mol Biol Evol 33:1635–1638

Iyer LM, Arvind L (2012) ALOG domains: provenance of plant homeotic and developmental regulators from the DNA-binding domain of a novel class of DIRS1-type retroposons. Biol Direct 7:39

Kohnen MV, Schmid-Siegert E, Trevisan M, Petrolati LA, Sénéchal F, Müller-Moulé P, Maloof J, Xenarios I, Fankhauser C (2016) Neighbor detection induces organ-specific transcriptomes, revealing patterns underlying hypocotyl-specific growth. Plant Cell 28:2889–2904

Kwok CS, Barris S, Burns J (2010) Increasing low light tolerance in plants. US Patent US2010/0119688A1. May 13

Lee J, Dong X, Choi K, Song H, Yi H, Hur Y (2020) Identification of source-sink tissues in the leaf of Chinese cabbage (*Brassica rapa* ssp. *pekinensis*) by carbohydrate content and transcriptomic analysis. Genes Genom 42:13–24

Li X, Sun L, Tan L, Liu F, Zhu Z, Fu Y, Sun X, Sun X, Xie D, Sun C (2012) *TH1*, a DUF640 domain-like gene controls lemma and palea development in rice. Plant Mol Biol 78:351–359

Lin T, Sharma P, Gonzalez DH, Viola IL, Hannapel DJ (2013) The impact of the long-distance transport of a *BEL1*-like messenger RNA on development. Plant Physiol 161:760–772

Liu C, Wang B, Li Z, Peng Z, Zhang J (2018) TsNAC1 is a key transcription factor in abiotic stress resistance and growth. Plant Physiol 176:742–756

Livak KJ, Schmittgen TD (2001) Analysis of relative gene expression data using real-time quantitative PCR and the $2^{-\Delta\Delta CT}$ method. Methods 25:402–408

Lorrai R, Boccaccini A, Ruta V, Possenti M, Costantino P, Vittorioso P (2018) Abscisic acid inhibits hypocotyl elongation acting on gibberellins. DELLA proteins and auxin. AoB Plants 10:ply061

MacAlister CA, Park SJ, Jinag K, Marcel F, Bendahmane A, Izkovich Y, Eshed Y, Lippman ZB (2012) Synchonization of the flowering transition by the tomato *TERMINATING FLOWER* gene. Nat Genet 44:1393–1398

Nguyen NH, Jeong CY, Kang GH, Yoo SD, Hong SW, Lee H (2015) MYBD employed by HY5 increases anthocyanin accumulation via repression of *MYBL2* in Arabidopsis. Plant J 84:1192–1205

Oh E, Zhu JY, Bai MY, Arenhart RA, Sun Y, Wang ZY (2014) Cell elongation is regulated through a central circuit of interacting transcription factors in the *Arabidopsis hypocotyl*. Elife 3:e03031

Press MO, Queitsch C (2017) Variability in a short tandem repeat mediates complex epistatic interactions in *Arabidopsis thaliana*. Genetics 205:455–464

Price MN, Dehal PS, Arkin AP (2009) FastTree: computing large minimum evolution trees with profiles instead of a distance matrix. Mol Biol Evol 26:1641–1650

Ramadoss N, Gupta D, Vaidya BN, Joshee N, Basu C (2018) Functional characterization of 1-aminocyclopropane-1-carboxylic acid oxidase gene in *Arabidopsis thaliana* and its potential in providing flood tolerance. Biochem Biophys Res Commun 503:365–370

Reed JW, Wu MF, Reeves PH, Hodgens C, Yadav V, Hayes S, Pierik R (2018) Three auxin response factors promote hypocotyl elongation. Plant Physiol 178:864–875

Shin J, Kim K, Kang H, Zulfugarov IS, Bae G, Lee CH, Lee D, Choi G (2009) Phytochromes promote seedling light responses by inhibiting four negatively-acting phytochrome-interacting factors. Proc Natl Acad Sci 106:7660–7665

Takeda S, Hanano K, Kariya A, Shimizu S, Zhao L, Matsui M, Tasaka M, Aida M (2011) CUP-SHAPED COTYLEDON1 transcription factor activates the expression of *LSH4* and *LSH3*, two members of the ALOG gene family, in shoot organ boundary cells. Plant J 66:1066–1077

Teo ZW, Song S, Wang YQ, Liu J, Yu H (2014) New insights into the regulation of inflorescence architecture. Trends Plant Sci 19:158–165

Tian T, Liu Y, Yan H, You Q, Yi X, Du Z, Xu W, Su Z (2017) agriGO v2.0: a GO analysis toolkit for the agricultural community, 2017 update. Nucleic Acids Res 45(W1):W122–W129

Trapnell C, Roberts A, Goff L, Pertea G, Kim D, Kelley DR, Pimentel H, Salzberg SL, Rinn JL, Pachter L (2012) Differential gene and transcript expression analysis of RNA-seq experiments with TopHat and Cufflinks. Nat Protoc 7:562–578

Tsukaya H (2013) Leaf Development. Arabidopsis Book 11:e0163

Vandenbussche F, Verbelen JP, Van Der Straeten D (2005) Of light and length: regulation of hypocotyl growth in Arabidopsis. BioEssays 27:275–284

Vernoux T, Brunoud G, Farcot E, Morin V, Van den Daele H, Legrand J, Oliva M, Das P, Larrieu A, Wells D, Guédon Y, Armitage L, Picard F, Guyomarc'h S, Cellier C, Parry G, Koumproglou R, Doonan JH, Estelle M, Godin C, Kepinski S, Bennett M, De Veylder L, Traas J (2011) The auxin signalling network translates

dynamic input into robust patterning at the shoot apex. Mol Syst Biol 7:508

Yan DW, Zhou Y, Ye SH, Zeng LJ, Zhang XM, He ZH (2013) *Beak-shaped grain 1/triangular hull 1*, a DUF640 gene, is associated with grain shape, size and weight in rice. Sci China Life Sci 56:275–283

Yoshida A, Suzaki T, Tanaka W, Hirano HY (2009) The homeotic gene *long sterile lemma* (*G1*) specifies sterile lemma identity in the rice spikelet. Proc Natl Acad Sci USA 106:20103–20108

Yoshida A, Sasao M, Yasuno N, Takagi K, Daimon Y, Chen R, Yamazaki R, Tokunaga H, Kitaguchi Y, Sato Y, Nagamura Y, Ushijima T, Kumamaru T, Iida S, Maekawa M, Kyozuka J (2013) *TAWAWA1*, a regulator of rice inflorescence architecture, functions through the suppression of meristem phase transition. Proc Natl Acad Sci USA 110:767–772

Yu G, Wang LG, Han Y, He QY (2012) clusterProfiler: an R package for comparing biological themes among gene clusters. Omics 16:284–287

Zhao L, Nakazawa M, Takase T, Manabe K, Kobayash M, Seki M, Shinozaki K, Matsui M (2004) Overexpression of *LSH1,* a member of an uncharacterised gene family, causes enhanced light regulation of seedling development. Plant J 37:694–706